Octaazacryptand Complexation of the Fluoride Ion

Sean D. Reilly, Guru Rattan K. Khalsa, Doris K. Ford, James R. Brainard, Benjamin P. Hay,† and Paul H. Smith*

Materials and Chemical Design Group, Chemical Science and Technology Division, CST-10, MS C346, Los Alamos National Laboratory, Los Alamos, New Mexico 87545

Received June 10, 1994[⊗]

The fundamental properties of proton, fluoride, and chloride binding of the octaazacryptand **L** have been investigated by potentiometry and NMR spectroscopy. Successive protonation constants of **L** are 11.18(16), 9.43(08), 7.59(07), 5.78(02), and 4.39(33), with the last value corresponding to a two-proton step. ^{1}H NMR spectra at 250 MHz indicate that proton exchange is slow on the NMR time scale in the pH region where the two-proton step occurs. It is proposed that this results from disruption of an internal hydrogen bond network and heightened electrostatic repulsions present in tetraprotonated **L**. NMR data also suggest that protonation occurs predominantly at the secondary amines over the pH range studied. Triprotonated **L** binds fluoride significantly (log $K = 3.6(4)$) near neutral pH, and further protonation of **L** increases the fluoride complex stability (log $K = 11.2(5)$ for the hexaprotonated fluoride complex). ^{1}H NMR data show that the rate of fluoride exchange decreases with solution pH. The magnitude of the aqueous fluoride binding constant, the substantial NMR shifts, and the published solid state structure suggest fluoride is bound inside the cavity of protonated **L**. MM2 calculations predict the strain energy of **L** increases by 10.2 kcal/mol when the expected nitrogen−halide hydrogen bond length increases from that of fluoride to that of chloride. Size selectivity of **L** is proposed to explain the fact that fluoride is bound over 10^7 times stronger than chloride.

Introduction

The molecular recognition of cations with specific geometric and electronic properties by macrocyclic receptors has been an area of extensive research over the past 25 years.[1−8] More recently, such receptors were designed to bind neutral molecules[9] and anions.[8,10−13] In contrast to the many donor functionalities available for cation binding, such as nitrogen, oxygen, sulfur, and phosphorus, anion coordination has relied heavily upon positively charged ammonium and guanidinium groups.

Of the halides, the fluoride ion provides a convenient target for the study of anion molecular recognition due to its tendency to form strong hydrogen bonds and its high hydration energy. Binding constants for the fluoride ion have been determined in solution with protonated tetraazamacrocycles[14] protonated and metalated octaaza- and octaazatrioxamacrobicycles,[15−17] a tin macrobicycle,[18,19] and porphyrin-related pentaazamacrocycles.[20−24] Activation enthalpies have been measured by NMR methods for fluoride binding with a fluorinated crown ether[25] and with (8-silyl-1-naphthyl)boranes,[26] neutral bidentate anion binders containing two different Lewis acid groups. In addition, NMR studies suggest that fluoride associates with an amide-functionalized macrobicyclic azacyclophane.[27] A macrocyclic phosphine oxide disulfoxide was recently reported which binds fluoride weakly.[28]

In the first paper describing the synthesis of **L**,[29] Dietrich[30] reported the X-ray crystallographic structure of a hexaprotonated cryptand−fluoride complex which provided evidence for the

† Present address: MS K6-82, Pacific Northwest Laboratory, P.O. Box 999, Richland, WA, 99352.

⊗ Abstract published in *Advance ACS Abstracts,* January 1, 1995.

(1) Lehn, J.-M. *Angew. Chem., Int. Ed. Engl.* **1988**, *27*, 89−112.
(2) Cram, D. J. *Angew. Chem., Int. Ed. Engl.* **1988**, *27*, 1009−1020.
(3) Pedersen, C. J. *Angew. Chem., Int. Ed. Engl.* **1988**, *27*, 1021−1027.
(4) *Cation Binding by Macrocycles*; Inoue, Y., Gokel, G. W., Eds.; Marcel Dekker: New York, 1990.
(5) Lindoy, L. F. *The Chemistry of Macrocyclic Ligand Complexes*; Cambridge University Press: Cambridge, U.K., 1989.
(6) Dietrich, B. In *Inclusion Compounds*; Atwood, J. L., Davies, J. E. D., MacNicol, D. D., Eds.; Academic Press: London, 1984; Vol. 2, pp 337−405.
(7) Izatt, R. M.; Bradshaw, J. S.; Nielsen, S. A.; Lamb, J. D.; Christensen, J. J.; Sen, D. *Chem. Rev.* **1985**, *85*, 271−339.
(8) Izatt, R. M.; Pawlak, K.; Bradshaw, J. S.; Bruening, R. L. *Chem. Rev.* **1991**, *91*, 1721−2085.
(9) Izatt, R. M.; Bradshaw, J. S.; Pawlak, K.; Bruening, R. L.; Tarbet, B. J. *Chem. Rev.* **1992**, *92*, 1261−1354.
(10) Dietrich, B. *Pure Appl. Chem.* **1993**, *65*, 1457−1464.
(11) Schmidtchen, F. P. *Nachr. Chem. Tech. Lab.* **1988**, *36*, 8−17.
(12) Pierre, J.-L.; Baret, P. *Bull. Soc. Chim. Fr.* **1983**, 367−380.
(13) Vögtle, F.; Sieger, H.; Müller, W. M. In *Host Guest Complex Chemistry I*; Vögtle, F., Ed.; Springer-Verlag: Berlin, 1981; Vol. 98, pp 107−161.
(14) Suet, E.; Handel, H. *Tetrahedron Lett.* **1984**, *25*, 645−648.
(15) Dietrich, B.; Guilhem, J.; Lehn, J.-M.; Pascard, C.; Sonveaux, E. *Helv. Chim. Acta* **1984**, *67*, 91−104.
(16) Motekaitis, R. J.; Martell, A. E.; Murase, I. *Inorg. Chem.* **1986**, *25*, 938−944.
(17) Motekaitis, R. J.; Martell, A. E.; Murase, I.; Lehn, J.-M.; Hosseini, M. W. *Inorg. Chem.* **1988**, *27*, 3630−3636.
(18) Newcomb, M.; Blanda, M. T. *Tetrahedron Lett.* **1988**, *29*, 4261−4264.
(19) Newcomb, M.; Horner, J. H.; Blanda, M. T.; Squattrito, P. J. *J. Am. Chem. Soc.* **1989**, *111*, 6294−6301.
(20) Sessler, J. L.; Cyr, M. J.; Lynch, V.; McGhee, E.; Ibers, J. A. *J. Am. Chem. Soc.* **1990**, *112*, 2810−2813.
(21) Sessler, J. L.; Ford, D. A.; Cyr, M. J.; Furuta, H. *J. Chem. Soc., Chem. Commun.* **1991**, 1733−1735.
(22) Shionoya, M.; Furuta, H.; Lynch, V.; Harriman, A.; Sessler, J. L. *J. Am. Chem. Soc.* **1992**, *114*, 5714−5722.
(23) Sessler, J. L.; Mody, T. D.; Ford, D. A.; Lynch, V. *Angew. Chem., Int. Ed. Engl.* **1992**, *31*, 452−455.
(24) Sessler, J. L.; Cyr, M.; Furuta, H.; Král, V.; Mody, T.; Morishima, T.; Shionoya, M.; Weghorn, S. *Pure Appl. Chem.* **1993**, *65*, 393−398.
(25) Farnham, W. B.; Roe, D. C.; Dixon, D. D.; Calabrese, J. C.; Harlow, R. L. *J. Am. Chem. Soc.* **1990**, *112*, 7707−7718.
(26) Katz, H. E. *J. Am. Chem. Soc.* **1986**, *108*, 7640−7645.
(27) Pascal, R. A., Jr.; Spergel, J.; Van Engen, D. *Tetrahedron Lett.* **1986**, *27*, 4099−4102.
(28) Savage, P. B.; Holmgren, S. K.; Gellman, S. H. *J. Am. Chem. Soc.* **1994**, *116*, 4069−4070.
(29) **L** = 1,4,7,10,13,16,21,24-octaazabicyclo[8.8.8]hexacosane.
(30) Dietrich, B.; Lehn, J.-M.; Guilhem, J.; Pascard, C. *Tetrahedron Lett.* **1989**, *30*, 4125−4128.

0020-1669/95/1334-0569$09.00/0

high structural complementarity of cryptand **L** for the fluoride

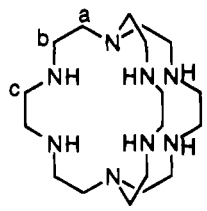

L

ion. Hunter[31] and Ragunathan[32] subsequently published studies of metal cation complexes with both **L** and an unsaturated Schiff base precursor. We recently described a simple two-step synthesis and the X-ray crystallographic structure of **L**.[33] Herein we report our studies of the proton, fluoride, and chloride binding properties of **L** using potentiometry and NMR spectroscopy. We demonstrate that cryptand **L** has an extremely high affinity for the fluoride ion in aqueous solution, a high selectivity for fluoride over chloride, and an H^+/F^- binding synergism which permits complete control of the degree of fluoride binding by **L**. We have used ^1H and ^{13}C NMR to study the structures of this cryptand and its fluoride complex and the dynamics of fluoride and proton exchange.

Experimental Section

Materials. **L** was synthesized in 47% overall yield using the previously reported procedure,[33] and its purity was verified by ^1H NMR and elemental analysis. Potassium hydroxide (carbonate free), hydrochloric acid, and nitric acid titrants were prepared from concentrates and ultrapure water to give 0.1 M solutions. The potassium hydroxide titrant was standardized with potassium hydrogen phthalate (99.95%), and the acid titrants were then standardized against the potassium hydroxide. A stock solution of 0.114 M tetramethylammonium fluoride ((TMA)F, 98%) was prepared and standardized with a stock sodium fluoride solution by standard addition. Stock 0.100 M sodium fluoride and 0.100 M sodium chloride solutions were used as received. The 0.10 M supporting electrolyte solutions of potassium nitrate, potassium chloride, and cesium bromide were prepared from reagent grade chemicals and ultrapure water. Dilution of 70% w/w DNO_3 (99% deuterated) with D_2O provided the 0.1 M DNO_3 solution. The 0.1 M NaOD solution was prepared by dilution of 40% w/w NaOD with D_2O.

Potentiometry. All potentiometric equilibrium measurements were conducted in a water-jacketed vessel at 25.0 ± 0.1 °C under ultrapure argon. The concentration of **L** in supporting 0.1 M electrolyte was approximately 0.002 M.[34] Titrants were dispensed using either a Metrohm 665 Dosimat or a Radiometer ABU93 Triburette. Potentiometric measurements were made using either an Orion Research EA940 pH meter or a Radiometer ABU93 Triburette. All buretes and pH meters were interfaced to a personal computer to permit automated data collection using software developed in this laboratory. A pK_w of 13.78 (0.10 M ionic strength, 25 °C) was used in all calculations.[35] Combination pH electrodes were calibrated before each titration as follows: Typically, 0.75 mL of standardized 0.1 M acid was added to 15 mL of supporting 0.1 M electrolyte. Standardized 0.1 M base was then titrated into the solution in ten 0.15 mL aliquots. The electrode potential was recorded before the titration and after the addition of each aliquot of base. Eleven data points were thereby collected over a pH range of 2.3−11.4. Linear least squares analysis of the electrode potential (in mV) as a function of the known acid concentration (below pH 3.0 and above pH 10.5) provided the electrode slope and intercept. This slope and intercept enabled the pH electrode to measure −log $[H^+]$ (designated p[H]) directly during subsequent titrations of cryptand **L**. Fluoride and chloride ion-specific electrodes were calibrated before cryptand−halide titrations as follows: Known amounts of fluoride ((TMA)F or NaF) or chloride (NaCl) were added to a solution of 0.1 M KNO_3 electrolyte while the electrode potential was recorded. Linear least squares analysis of the electrode potential as a function of halide concentration enabled the electrodes to measure −log $[F^-]$ and −log $[Cl^-]$ (designated p[F] and p[Cl], respectively).

Cryptand **L** in KNO_3 electrolyte was titrated with HNO_3 while the p[H] was measured. Three separate titrations were performed, and 173−176 data points were collected in the p[H] range 2.2−11.0 for each data set. Overall cryptand protonation constants (log β) were determined separately for each data set by nonlinear least squares analysis of the data using the computer program BETA.[36] A weighted average value of each stepwise protonation constant (log K^H_n) was calculated using the equation

$$\log K = \{\sum_{i=1}^{n}[(\log K)_i/\sigma_i^2]\}/\{\sum_{i=1}^{n}(1/\sigma_i^2)\}$$

where values of σ were obtained from BETA and the sum is over n repetitions. The error in log K is reported as the standard deviation of the $(\log K)_i$ values and thus represents the reproducibility of titration results. Potentiometric equilibrium measurements of **L**−fluoride complexes were determined by titrating a 1:1 **L**:(TMA)F solution in KNO_3 electrolyte with HNO_3 while both p[H] and p[F] were measured. Two titrations were performed, and 145−154 data points were collected in the p[H] range 3.3−10.9 for each data set. Analysis of the p[H] data from these titrations using BETA provided overall formation constants (log β) of four **L**−fluoride complexes.[37] The weighted average values and associated errors of log β_{FLH_3} (31.8(3)) and each log $K^H_{FLH_n}$ (Table 1) were calculated as described above. The stepwise fluoride binding constants (log K_{FLH_n}) in Table 1 were derived from the corresponding log β_{LH_n} and log β_{FLH_n} values. In a separate experiment to further elucidate fluoride complexation behavior, p[H] and p[F] were measured as NaF was titrated into an acidic solution of **L** in KNO_3 electrolyte. For the chloride binding constant determination, cryptand **L** in KCl electrolyte was titrated with HCl while the p[H] was measured.[38] The weighted average and associated error for the chloride binding constant log β_{ClLH_5} (37.36(12)) were calculated on the basis of seven such titrations, with each data set containing 168−198 data points collected over a p[H] range of 2−11. In a separate experiment, NaCl was titrated into an acidic solution of **L** in KNO_3 electrolyte while p[H] and p[Cl] were measured.

NMR Spectroscopy. ^1H and ^{13}C NMR spectra were acquired on IBM AF-250 and Bruker AM-200 NMR spectrometers, and chemical shifts are reported relative to TSP in D_2O. A 2 Hz exponential line broadening was applied to ^{13}C NMR fid's prior to Fourier transformation. An Orion EA 920 pH meter and an Ingold combination pH electrode for NMR tubes were utilized in making pH measurements. Standard pH 4, 7, and 10 buffers in H_2O were employed in calibrating the electrode. Uncorrected pH meter readings are designated pH*.

(31) Hunter, J.; Nelson, J.; Harding, C.; McCann, M.; McKee, V. *J. Chem. Soc., Chem. Commun.* **1990**, 1148−1151.
(32) Ragunathan, K. G.; Bharadwaj, P. K. *J. Chem. Soc., Dalton Trans.* **1992**, 1653−1656.
(33) Smith, P. H.; Barr, M. E.; Brainard, J. R.; Ford, D. K.; Freiser, H.; Muralidharan, S.; Reilly, S. D.; Ryan, R. R.; Silks, L. A., III; Yu, W.-h. *J. Org. Chem.* **1993**, *58*, 7939−7941.
(34) Cryptand **L** is recrystallized from water, and its hydration state varies. The concentration of **L** was determined by calculating the derivative, d(titrant volume)/d(p[H]) and assuming that its lowest minimum corresponds to 4 equiv of added acid titrant.
(35) Smith, R. M.; Martell, A. E. *Critical Stability Constants*; Plenum Press: New York, 1989; Vol. 6.
(36) Harris, W. R.; Raymond, K. N. *J. Am. Chem. Soc.* **1979**, *101*, 6534−6541. BETA requires estimates of the intrinsic error in the buret (σ_v) and the pH meter (σ_{meter}). The protonation and fluoride binding constants reported here were computed using σ_v = 0.015 mL and σ_{meter} = 0.03 pH unit, and the chloride binding constant was computed using σ_v = 0.01 mL and σ_{meter} = 0.03 pH unit.
(37) We included the association constants for HF (K = [HF]/[H][F], log K = 2.94) and HF_2 (K = $[HF_2]$/[HF][F], log K = 0.57) obtained from ref 35 when refining the **L**−fluoride binding constants and calculating the species plot in Figure 4. Due to the high fluoride affinity of protonated **L**, formation of HF and HF_2 is not observed.
(38) Titration curves of **L** in KNO_3 at a 1:1 **L**:Cl^- ratio were identical to those obtained in KNO_3 alone. Therefore, the chloride binding constant was determined using KCl as the supporting electrolyte, and the total chloride concentration used in the calculation was 0.11 M.

Table 1. Stepwise Protonation Constants[a] and Fluoride[a] and Chloride[b] Binding Constants for Cryptand **L**

n	equilibrium K^{H}_{n}	log K^{H}_{n}	equilibrium $K^{H}_{FLH_n}$	log $K^{H}_{FLH_n}$	equilibrium K_{XLH_n}	log K_{XLH_n} X = F^-	log K_{XLH_n} X = Cl^-
1	[LH]/[L][H]	11.18(16)[c]					
2	$[LH_2]/[LH][H]$	9.43(08)					
3	$[LH_3]/[LH_2][H]$	7.59(07)			$[XLH_3]/[LH_3][X]$	3.6(4)	
4	$[LH_4]/[LH_3][H]$	5.78(02)	$[FLH_4]/[FLH_3][H]$	7.31(03)	$[XLH_4]/[LH_4][X]$	5.1(4)	
5			$[FLH_5]/[FLH_4][H]$	5.89(05)	$[XLH_5]/[LH_5][X]$[d]	≥8.8(4)	≥1.2(3)
6	$[LH_6]/[LH_4][H]^2$	4.39(33)	$[FLH_6]/[FLH_5][H]$	4.56(04)	$[XLH_6]/[LH_6][X]$	11.2(5)	

[a] 0.1 M KNO_3, 25.0 °C. [b] 0.1 M KCl, 25.0 °C. [c] Numbers in parentheses are the standard deviations in the least significant figures. [d] Reference 65 lists values for log β_{FLH_5} and log β_{ClLH_5}. The estimates for log K_{XLH_5} were obtained by assuming the two-proton step, $LH_4 + 2H^+ \rightleftharpoons LH_6$, could be broken down into two single-proton equilibria, in which the first is ≤4.39/2, and their sum is 4.39.

Solutions of cryptand (~25 mM initial concentration) were prepared in 0.1 M KNO_3, KCl, or KF in D_2O. Solution pH was adjusted with DNO_3, DCl, or NaOD. For the constant-pH fluoride titrations, the fluoride concentration of the solutions was adjusted through addition of a solution of KF in D_2O, and the pH was readjusted after each addition of KF.

The ^1H spectrum of **L** at pH* 11.29 exhibits resonances at δ 2.82 (s), 2.72 (m), and 2.55 (m) ppm. The singlet at 2.82 ppm is unequivocally assigned to H_c. Protons H_a (2.55 ppm) and H_b (2.72 ppm) are assigned on the basis of comparison to 1-methylpiperazine[39] and to N-methylated ethylenediamines.[40] Carbon assignments of **L** at pH* 4.4 [δ 54.0 (C_a), 49.2 (C_c), 48.9 (C_b) ppm], pH* 5.5 [δ 54.2 (C_a), 49.5 (C_c), 49.0 (C_b) ppm], and pH* 11.3 [δ 55.5 (C_a), 51.6 (C_c), 49.3 (C_b) ppm] are based on selective $^1H-^{13}C$ decoupling experiments. Selective decoupling experiments in the presence of fluoride ion were conducted at pH* 4.4 [δ 53.0 (C_a), 48.9 (C_b), 48.2 (C_c) ppm] and pH* 5.3 [δ 53.2 (C_a), 48.9 (C_b), 48.8 (C_c) ppm]. These carbon and proton assignments are further supported by the fact that carbons α to tertiary amines resonate further downfield than those α to secondary amines.[41]

Molecular Mechanics. Molecular mechanics calculations were performed to determine the optimum cavity size for metal ion complexation by the unprotonated ligand. The conformation observed in the crystal structures of both the free ligand[33] and the fluoride complex[30] was used, and this is the expected conformation for minimum strain coordination of an anion. In these calculations, only the six secondary amines were bonded to the metal, as observed in the fluoride cryptate structure. To accomplish this, energy minimizations were carried out as a function of M–N bond length at 0.1 Å intervals from 1.9 to 3.6 Å by fixing the M–N bond lengths to the desired value and setting their stretching force constant to 99 mdyn/Å.[42-44] Molecular mechanics calculations were performed with the MM2 program.[45] Input files were modified to allow the number of attachments to the metal atom to be greater than 4.[46] The input files were also modified to reproduce the model used in other calculations of transition metal–amine complexes.[47-49] These modifications included the replacement of N–M–N bond angles with N to N nonbonded interactions, setting the MM2 cubic stretch and stretch–bend terms to zero and assigning metal-dependent parameters.[47-49] The program Chem3D Plus[50] was used to build initial sets of molecular coordinates and to plot the energy-minimized molecular coordinates obtained from the calculations.

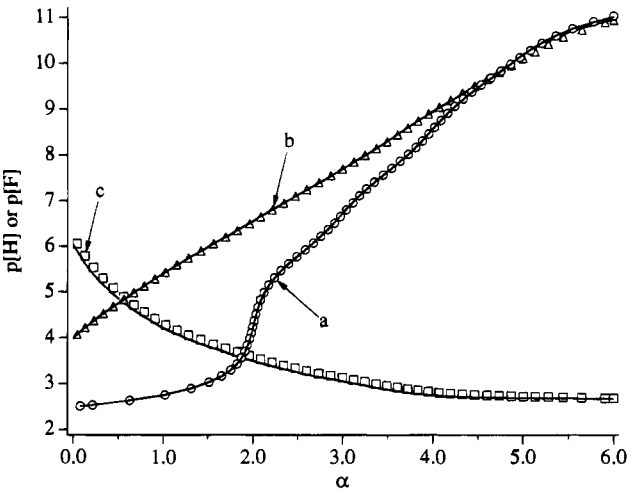

Figure 1. Potentiometric p[H] titrations of **L** in the absence (curve a) and presence of fluoride ion (curve b). Ion-selective-electrode p[F] measurements in the presence of fluoride ion are shown as curve c. Circles, triangles, and squares indicate observed data while lines show calculated data. α is defined as mmol of base/mmol of **L**. For clarity, only every third data point is shown.

Results and Discussion

Cryptand Protonation. Cryptand **L** is a polyfunctional base, and consequently the extent of protonation increases as solution pH decreases. Protonation constants for **L** were derived from potentiometric p[H] titration data[51] (Figure 1, curve a circles) and are listed in Table 1. The species distribution diagram in Figure 2 illustrates the p[H] ranges over which the various cryptand protonation states exist. Since **L** possesses eight nitrogen atoms, it could be expected to bind up to eight protons to give the species LH_8.[52] However, under the employed experimental conditions LH_6 is the most protonated form of the ligand observed. Curve a of Figure 1 is best fit using a model in which the sixth protonation of **L** is coincident with the fifth. Therefore, the equilibrium K^{H}_{6} shown in Table 1 is formulated to involve two protons and no value for log K^{H}_{5} is listed.[53] Published protonation constants for cyclam and one of its tetrasubstituted derivatives include analogous two-proton equilibria.[54-56]

(39) Pretsch, E.; Clerc, T.; Seibl, J.; Simon, W. *Tables of Spectral Data for Structure Determination of Organic Compounds*, 2nd ed.; Springer-Verlag: Berlin, 1989.
(40) Sudmeier, J. L.; Reilley, C. N. *Anal. Chem.* **1964**, *36*, 1698–1706.
(41) Breitmaier, E.; Voelter, W. *Carbon-13 NMR Spectroscopy: High-Resolution Methods and Applications in Organic Chemistry and Biochemistry*, 3rd ed.; VCH Verlagsgesellschaft: New York, 1987; pp 121, 236–238.
(42) Drew, M. G. B.; Hollis, S.; Yates, P. C. *J. Chem. Soc., Dalton Trans.* **1985**, 1829–1834.
(43) Drew, M. G. B.; Yates, P. C. *Pure Appl. Chem.* **1989**, *61*, 835–840.
(44) Bell, T. W.; Guzzo, F.; Drew, M. G. B. *J. Am. Chem. Soc.* **1991**, *113*, 3115–3122.
(45) Allinger, N. L.; Yuh, Y. H. *MM2, Quantum Chemistry Program Exchange*, modified version; Indiana University Chemistry Department: Bloomington, IN, 1980; QCPE Program No. 395.
(46) Hay, B. P. *Inorg. Chem.* **1991**, *30*, 2876–2884.
(47) Hambley, T. W.; Hawkins, C. J.; Palmer, J. A.; Snow, M. R. *Aust. J. Chem.* **1981**, *34*, 45–56.
(48) Bond, A. M.; Hambley, T. W.; Snow, M. R. *J. Am. Chem. Soc.* **1985**, *24*, 1920–1928.
(49) Snow, M. R. *Inorg. Chem.* **1970**, *92*, 3610–3617.
(50) Rubenstein, M.; Rubenstein, S. *Chem3D Plus*; Cambridge Scientific Computing, Inc.: Cambridge, MA, 1989.
(51) Protonation constants determined in CsBr electrolyte are similar to those determined in KNO_3. On the basis of the expectation that Cs^+ and Br^- are bound only weakly to the cryptand, we have assumed that neither K^+ nor NO_3^- binds to **L** significantly.
(52) Throughout this paper, charges have been omitted for clarity, and the free base **L** is a neutral molecule.

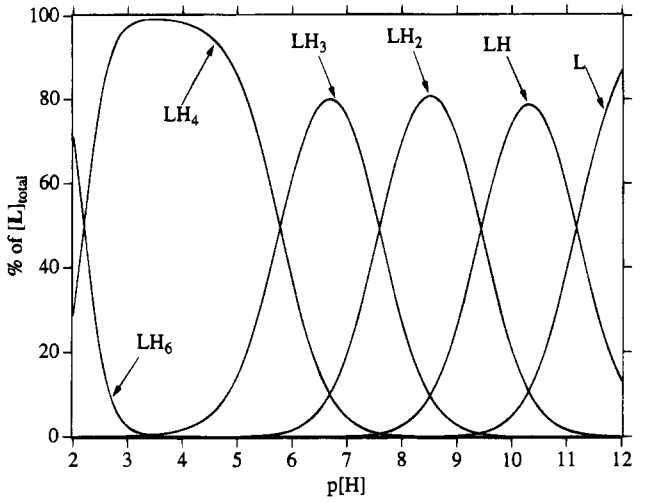

Figure 2. Species plot showing the protonation states of **L** as a function of p[H] where $[\mathbf{L}]_{total}$ is 2 mM.

The unprotonated cryptand **L** is a strong base, as indicated by the high value of log K^{H}_{1}. Protonation constants log K^{H}_{2-4} steadily decrease in magnitude, reflecting a decrease in the basicity of **L** with each subsequent protonation. This decline is well established for polyazamacrocycles and is usually attributed to electrostatic and statistical factors which depend on structural aspects including amine spacing and macrocycle size.[57,58] Figures 1 and 2 indicate that the protonation of LH_4 is qualitatively different from the earlier protonation steps. This is illustrated by the wide p[H] range of 5.8−2.8 over which LH_4 exists (see Figure 2 and the sharp breakpoint in curve a, Figure 1, at $\alpha = 2.0$). Thus, protonation occurs in two distinct phases: a high-pH phase (L−LH_4, above pH 4) and a low-pH phase (LH_4−LH_6, below pH 4).

The shift in cryptand resonances with pH was followed by ^{1}H NMR (Figure 3). These data were evaluated using the method of Sudmeier and Reilley,[40] whereby chemical shifts are used to predict the percentage of protonation at secondary and tertiary amine sites. Whereas the significance of this method must be tempered by its applicability to conformationally restricted polyamines, the results suggest that secondary amines are protonated almost exclusively in LH through LH_6. These NMR results also emphasize the distinct protonation behaviors above and below pH ~4. As pH* decreases from 8.8 to 3.6 in Figure 3, the protonation state of **L** progresses from LH_2 to LH_4. A gradual downfield shift in all resonances is observed in this pH region, and proton exchange is fast on the NMR time scale. As the pH decreases further, three new ^{1}H resonances grow in and eventually replace the original resonances. Significant broadening in this pH region indicates that protonation is in intermediate exchange on the NMR time scale. This pH range corresponds to the protonation of LH_4 to give LH_6 (Figure 2).

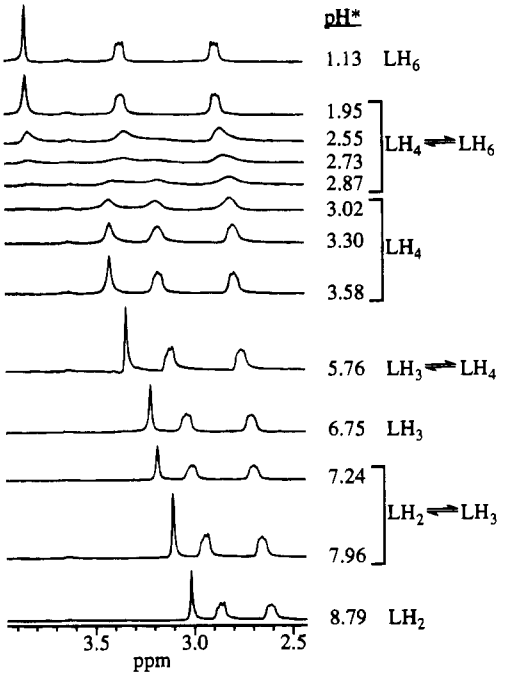

Figure 3. pH titration of cryptand **L** with DCl in 0.1 M KCl monitored by 250 MHz ^{1}H NMR. The cryptand protonation states as determined from Figure 2 are listed at right.

Protonation of **L** causes upfield shifts of the ^{13}C NMR resonances: $\Delta\delta$ −1.2 (C_a), -0.2 (C_b), −2.4 (C_c) ppm as pH* varies from 11.39 to 2.43. In the ^{13}C spectra, amine protonation generally results in the upfield shift of substituent alkyl carbons, particularly carbons β to the protonated amine.[41,59] The ^{13}C resonance of C_c shifts the most, suggesting that it is the carbon most affected by amine protonation in this pH region. Because C_c is the only carbon both β and α to secondary amines, the large upfield shift in its resonance suggests that initial protonation occurs primarily at the secondary amines. The less pronounced upfield shift of C_a, which is β (but not α) to a secondary amine, is also consistent with secondary amine protonation. The resonance of C_b is shifted the least because it is only α to secondary amines. These ^{13}C NMR observations further support the conclusion that amine protonation from LH to LH_6 occurs predominantly at the secondary amines.

Simple electrostatic arguments would suggest that at least one tertiary amine would be protonated in LH_{4-6} to maximize the distance between positive charges. Thus, the preferential protonation of the secondary amines through LH_6 appears to contradict expectations based on electrostatic considerations alone. The observation of two distinct phases of protonation also requires some explanation. We propose that above pH 4 the secondary amines are oriented internal to the cryptand cavity and participate in an intramolecular hydrogen bond network. Upon protonation of LH_4 below pH 4, this hydrogen bond network is at least partially disrupted, and the cryptand undergoes a major conformational change involving outward rotation of the secondary amines to reduce electrostatic repulsions.

Evidence for this hypothesis begins with the reported crystal structure of the cryptand.[33] The cryptand was crystallized from a high-pH aqueous solution, and the secondary amines are hydrogen-bonded to a surrounding network of water molecules. The lone pairs of the tertiary amines are directed into the cavity, thus shielding them from significant interaction with solvent

(53) Separate stepwise protonation constants for LH_5 and LH_6 could be refined, but they were highly and inversely correlated. A species distribution diagram computed from these values indicated that the concentration of LH_5 in solution is negligible; its maximum concentration never exceeds 5% of the total concentration of **L**.

(54) Micheloni, M.; Sabatini, A.; Paoletti, P. *J. Chem. Soc., Perkin Trans. 2* **1978**, 828−830.
(55) Thöm, V. J.; Hosken, G. D.; Hancock, R. D. *Inorg. Chem.* **1985**, *24*, 3378−3381.
(56) Tan, L. H.; Taylor, M. R.; Wainwright, K. P.; Duckworth, P. A. *J. Chem. Soc., Dalton Trans.* **1993**, 2921−2928.
(57) Kimura, E. In *Biomimetic and Bioorganic Chemistry*; Boschke, F. L., Ed.; Springer-Verlag: Berlin, 1985; Vol. 128; pp 113−144.
(58) Bianchi, A.; Micheloni, M.; Paoletti, P. *Coord. Chem. Rev.* **1991**, *110*, 17−113.
(59) Sarneski, J. E.; Surprenant, H. L.; Molen, F. K.; Reilley, C. N. *Anal. Chem.* **1975**, *47*, 2116−2124.

water molecules. In the structure the N−H protons are directed toward the center of the cavity, and the range of adjacent N−N distances is 2.93−3.04 Å, which is well within the range of typical N−H···N hydrogen bonds. These data are consistent with a high-pH solution conformation in which the tertiary amine lone pairs and the secondary amine hydrogens are directed into the cavity. The ^{1}H NMR data provide strong evidence for a substantial conformational change upon protonation of LH_4, given that proton exchange slows and the resonances shift the most between LH_4 and LH_6.[60] We propose that this conformational change breaks the internal hydrogen bonds and rotates the amines external to the cavity. The conformational change helps to reduce electrostatic repulsions and simultaneously enables increased internal van der Waals interactions of the hydrocarbon chains. The observed two-proton step is likely a result of the concomitant disruption of the internal hydrogen bond network. The resistance to further protonation of diprotonated cyclam[54,61] and a small monoprotonated aza cage molecule[62] has been similarly attributed to internal hydrogen bonds. The greater accessibility of the secondary amines suggests that positive charges on protonated secondary amines can be more effectively dissipated to the solvent through hydrogen bonds. Thus, favorable solvation, hydrogen-bonding effects, and the conformational change itself compensate for electrostatic repulsions and account for preferential secondary amine protonation.

Fluoride and Chloride Binding. Titration of a stoichiometric mixture of **L** and (TMA)F with HNO_3 proceeded while two different electrodes were used to simultaneously measure both p[H] and p[F] (Figure 1, curves b and c, respectively).[63] This method provides two independent measures of key solution species (free H^+ and F^-) as a function of added titrant. A model which includes the previously determined protonation constants and four fluoride complexes FLH_{3-6} was used to fit the p[H] data,[36] and the log K_{FLH_n} values are listed in Table 1.[64] In turn, these constants were used to calculate solution p[F] as a function of α (Figure 1, solid line of curve c). The close agreement between this calculated p[F] curve and the aforementioned observed p[F] curve is further indication that the binding constants determined from the p[H] data provide an accurate model of the species in solution. The protonation and fluoride stability constants in Table 1 predict the p[H]-dependent solution speciation of cryptand and fluoride complexes plotted in Figure 4.[37]

The fact that curve b lies above curve a for α = 0−4 in Figure 1 indicates that protonation of **L** is more favorable in the presence of fluoride in this pH range. The values of the protonation constants (log $K^H_{FLH_n}$) for **L**−fluoride complexes are listed in Table 1. Comparison of the affinities of LH_3 and FLH_3 for protons indicates that fluoride binding increases this affinity by a factor of $10^{1.53}$. A similar comparison of the diprotonation of LH_4 and FLH_4 reveals an increase by a factor of $10^{6.1}$. The following equations further illustrate these comparisons and demonstrate the synergistic binding of protons

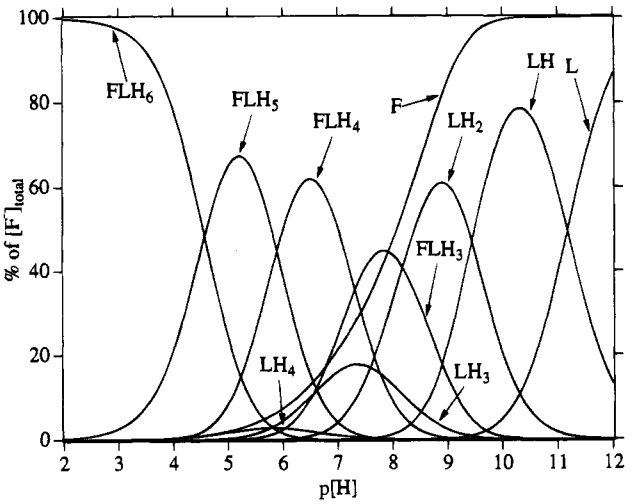

Figure 4. Species plot showing the cryptand−fluoride complexes as a function of p[H] where $[L]_{total} = [F^-]_{total} = 2$ mM.

and fluoride ion in the cryptand:

$$[FLH_3]^{2+} + [LH_4]^{4+} \rightleftharpoons [FLH_4]^{3+} + [LH_3]^{3+} \quad \log K = 1.53(03)$$

$$[FLH_4]^{3+} + [LH_6]^{6+} \rightleftharpoons [FLH_6]^{5+} + [LH_4]^{4+} \quad \log K = 6.1(3)$$

These equilibria also emphasize the increasing fluoride affinity as the degree of protonation increases. Examination of the species plots (Figures 2 and 4) reveals that the maximum concentration of LH_4 occurs at pH 3.5 while the maximum concentration of FLH_4 occurs at pH 6.5. This cooperative H^+/F^- binding provides for total reversibility of the extent of fluoride binding through pH adjustment.

Determination of the **L**−chloride binding constant is complicated due to the low affinity of the cryptand for chloride. As a result, the binding constant could not be determined under stoichiometric conditions. However, the $ClLH_5$ binding constant could be determined in the presence of a 55-fold excess of chloride. This value is listed in Table 1. A value for log K_{ClLH_6} could not be computed from the data. Because the two-proton step between LH_4 and LH_6 discussed above precludes determination of log K^H_5, Table 1 lists only the lower limits to the chloride and fluoride binding constants log K_{XLH_5}. The equilibrium expression for F^-/Cl^- exchange is shown in the following equation:[65]

$$[ClLH_5]^{4+} + F^- \rightleftharpoons [FLH_5]^{4+} + Cl^- \quad \log K = 7.6(3)$$

Thus, the cryptand exhibits 7 orders of magnitude selectivity for fluoride over chloride.

Figure 5 illustrates further the strength of fluoride complexation in comparison to chloride. As NaF is titrated into a solution of **L** at low p[H], p[F] (curve a) remains high before the breakpoint at α =1, indicating that the first equivalent of fluoride is strongly bound by **L** to form a 1:1 fluoride complex.[66] Also evident at α = 1 is a sharp discontinuity in the p[H] curve (curve b). This significant increase in p[H] as fluoride is added up to α = 1 illustrates the cooperative H^+/F^- binding referred

(60) Similar results are observed in both Cl^- and NO_3^- media with slightly different chemical shifts.
(61) Micheloni, M.; Paoletti, P.; Vacca, A. *J. Chem. Soc., Perkin Trans. 2* **1978**, 945−947.
(62) Ciampolini, M.; Micheloni, M.; Vizza, F.; Zanobini, F.; Chimichi, S.; Dapporto, P. *J. Chem. Soc., Dalton Trans.* **1986**, 505−510.
(63) No significant interaction between **L** and the tetramethylammonium cation is expected.
(64) Use of p[H] data to determine the fluoride binding constants is preferable to using p[F] data because the p[H] range where the fluoride species are important is well within the accurate operating range of a p[H] electrode, whereas the p[F] range approaches the lower limit of fluoride ion detection of the fluoride electrode.
(65) The values for the overall formation constants $\beta_{XLH_5} = [XLH_5]/[LH_5][X]$ (where X is F^- or Cl^-) are log $\beta_{FLH_5} = 45.0(3)$ and log $\beta_{ClLH_5} = 37.36(12)$.
(66) **L** is expected to bind Na^+ at high p[H], but not in the acidic p[H] range of this experiment. NaF was therefore used in lieu of (TMA)F because the former may be obtained as a primary standard.

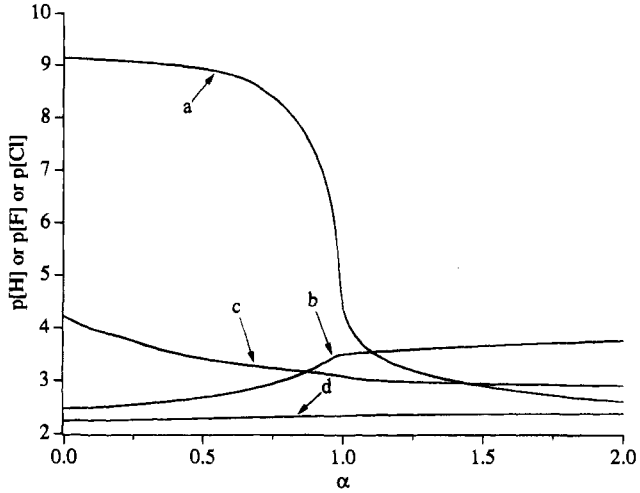

Figure 5. Potentiometric titrations of **L** with fluoride ion (curve a, p[F]; curve b, p[H]) or chloride ion (curve c, p[Cl]; curve d, p[H]). α is defined as mmol of halide/mmol of **L**.

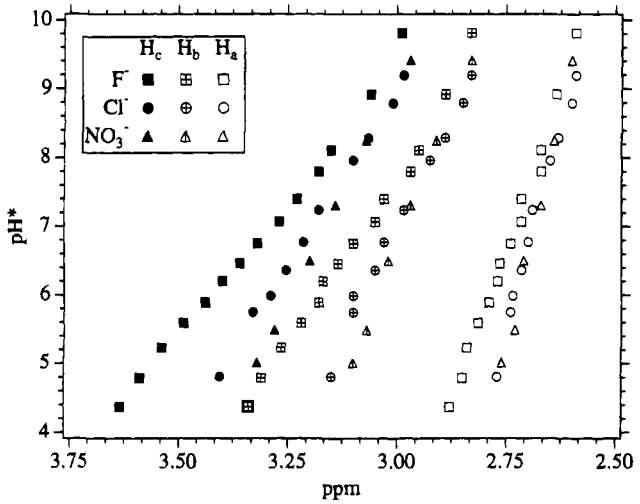

Figure 6. pH titrations of cryptand **L** in 0.1 M KF, KCl, and KNO_3 monitored by 250 MHz ^1H NMR.

to above. Once the cryptand−fluoride complex is formed, further addition of fluoride beyond $\alpha = 1$ causes only very small changes in p[H]. Fluoride in excess of 1 equiv ($\alpha > 1$) exists unbound in solution, as indicated by the low p[F]. This is consistent with the 1:1 fluoride cryptate observed in the crystal structure.[30] When NaCl is titrated into a solution of **L** at low p[H], the p[Cl] curve (curve c) is much lower than the p[F] curve (curve a) up to $\alpha = 1$ and has no sharp breakpoint. This is in sharp contrast to the p[F] curve (curve a). Similarly, there is no discontinuity in the p[H] curve (curve d). Thus, there is no evidence for the formation of a robust chloride complex.

The relative shifts of the ^1H resonances as a function of pH* in 0.1 M KNO_3, 0.1 M KCl, and 0.1 M KF are depicted in Figure 6. The ^1H resonances of **L** shift the least in the presence of NO_3^- on adjustment of pH from high (where no binding of anions to cryptand occurs) to low values (where anions may bind). Slightly greater changes in ^1H chemical shifts are seen for **L** in 0.1 M KCl relative to those for **L** in 0.1 M KNO_3, indicating that the chloride ion binds to protonated cryptand more strongly than the nitrate ion. Substantially larger changes in chemical shift are observed for cryptand in 0.1 M KF as pH is lowered, reflecting the stronger binding of fluoride to cryptand. Above pH* 9, the chemical shifts of the three proton resonances are essentially the same in all three electrolytes. This supports the model represented in the speciation plot (Figure 4), which indicates that fluoride is not bound to **L** at pH 10. As the pH is lowered, **L** becomes increasingly protonated and thereby more able to bind anions. Thus, the relative strength of interaction of **L** with the respective anions becomes more apparent by ^1H NMR as pH is lowered.

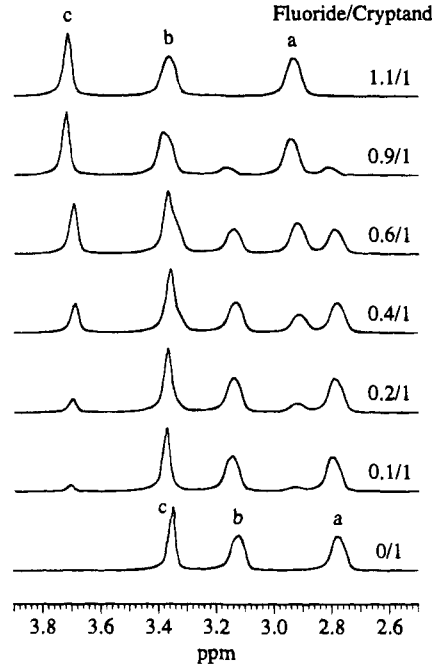

Figure 7. Titration of cryptand with KF at pH* 4.0 ± 0.1 monitored by 250 MHz ^1H NMR. Letters above resonances refer to proton assignments of **L**, and the fluoride:cryptand ratio is listed at right.

Incremental additions of fluoride to solutions of cryptand were followed by ^1H NMR spectroscopy while pH* was maintained at 4.0, 5.5, and 7.3. The spectra at pH* 4.0 are illustrated in Figure 7. As fractional equivalents of fluoride are added, new resonances proportionately grow into the ^1H NMR spectra as the three resonances due to free cryptand disappear. Here the proton resonances for free and fluoride-bound cryptand are in slow exchange on the NMR time scale. ^1H NMR at pH* 5.5 suggest intermediate exchange while at pH* 7.3 exchange is fast. The progression from slow to fast exchange with increasing pH corresponds with the decreasing cryptand affinity for fluoride. Other heteronuclear NMR studies are in progress to further elucidate the exchange behavior.

We have used molecular mechanics calculations to estimate the strain energy of **L** as a function of cavity size. The results of the modeling study are illustrated in Figure 8, where the total strain energy is plotted as a function of M−N distance from 1.9 to 3.6 Å. Conformational integrity was verified by generating Chem3D Plus views from the MM2 output files of the energy-minimized structures. This same geometry achieves the expected configuration for minimum strain coordination of an anion by the fully protonated form of the ligand where all N−H···F bonds would be close to linear. The minimum strain energy for this conformation of the ligand occurs at a M−N distance of 2.91 Å. It is interesting to note that the optimum M−N distance predicted by these calculations is nearly identical to the median N−F distance of 2.81 Å observed in the FLH_6 crystal structure.[30] This is not surprising, given that the minimum strain cavity size for metal ion complexation occurs when the nitrogen donor groups are closest to their desired tetrahedral geometry with lone pairs oriented toward the center of the cavity. The predicted increase in strain energy from the fluoride cryptate N−F distance of 2.81 Å to the average N−Cl distance of 3.23 Å is 10.2 kcal/mol, suggesting that, in this

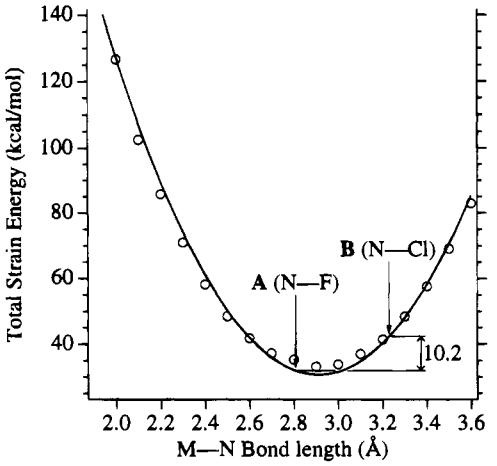

Figure 8. Strain energy of cryptand **L** as a function of metal−nitrogen bond length calculated by MM2 (circles). The solid line is the best-fit line: strain energy = 1013.8 − 674.95(M−N bond length) + 115.85-(M−N bond length)^2. Point A is the median N−F hydrogen bond length in the FLH_6 fluoride cryptate crystal structure[30] and point B is a typical N−Cl hydrogen bond length.[15]

conformation, **L** exhibits a significant steric preference for fluoride ion over chloride ion.

The demonstrated selectivity and the extraordinary binding constant of the cryptand are largely due to an ideal cavity size match and to the small size of fluoride relative to the other halide ions. The small size of fluoride gives rise to strong fluoride hydrogen bonds and thus short hydrogen bond lengths (2.92 Å for F−N vs 3.23 Å for Cl−N)[15] and to a high hydration energy (−103.8 kcal/mol for F^- vs −75.8 kcal/mol for Cl^-).[67] Also, the total charge on the cryptand is an extremely important factor. As successive protons are added to the cryptand−fluoride complex, they significantly enhance the binding of fluoride, and the fluoride ion likely reduces the charge repulsion in the protonated cryptand. This effect becomes more pronounced at lower pH's, where the cryptand is more highly protonated. The cryptand provides as many as six positive charges in ideal positions for hydrogen bonding and thus presents an optimal environment to the fluoride ion.

Comparison of the magnitude of the **L**−fluoride binding constants with those of other cryptands and nitrogen macrocycles indicates that **L** is exceptionally well suited to bind fluoride. Previously, the highest reported aqueous fluoride−cryptand association constant was for hexaprotonated O-BISTREN (log $K_{FLH_6} = 4.1$).[15] The larger fluoride binding constant of **L** is attributed to the improved fit of fluoride in its smaller cavity. The highest reported macrocycle association constant measured in nonaqueous media is for the expanded porphyrin sapphyrin (log $K_{FLH_2} > 10^8$).[22] Differences in fluoride solvation in organic solvents greatly influence binding affinity and preclude direct comparison with aqueous systems.

Conclusion

Dietrich's crystal structure of the fluoride cryptate[30] and the magnitude of the fluoride binding constant for LH_6 measured here strongly suggest that the fluoride ion binds inside the cryptand cavity in aqueous solution. Comparison of the proton NMR data for the cryptand which show large shifts upon addition of fluoride and small shifts upon addition of chloride (relative to nitrate) suggest that chloride does not bind inside the cryptand cavity. The low binding constant for chloride and the increase in strain energy of the ligand predicted upon chloride binding further support this conclusion. Dietrich's crystal structure illustrates a median N−F distance of 2.81 Å, which is typical of N−H···F hydrogen bonds, and the distance from the cavity center to all secondary amines in the crystal structure of the free ligand is 2.82 Å. Thus, the selectivity is primarily associated with the ideal match of the cryptand cavity with the size of the fluoride ion.

The overall magnitude of fluoride binding ($10^{11.2}$) and the fluoride/chloride selectivity ($10^{7.6}$) of this cryptand in water are unprecedented. The pH-controlled reversibility of fluoride binding in the cryptand system (see curve F in Figure 4) yields an important advantage when applications in separations chemistry are considered. We are in the process of covalently attaching this cryptand to polymeric materials to explore potential applications. We are also derivatizing the secondary amines to explore the effects on anion and metal binding.

Acknowledgment. Funding for this research has been provided by the U.S. Department of Energy under the Laboratory Directed Research and Development Program. G.R.K.K. gratefully acknowledges the award of a faculty sabbatical fellowship from the Associated Western Universities/U.S. Department of Energy. We wish to thank Dr. Mary P. Neu for valuable discussions.

IC9406695

(67) Free energies of solvation for the process $X^-(g) \rightarrow X^-(aq)$ are −103.8 and −75.8 kcal/mol for $X^- = F^-$ and Cl^-, respectively: Goldman, S.; Bates, R. G. *J. Am. Chem. Soc.* **1972**, *94*, 1476−1484.